COMMUNICATIONS IN APPLIED NUMERICAL METHODS, Vol. 4, 741–748 (1988)

A COMPARISON OF SOLUTIONS FOR ADIABATIC SHEAR BANDING BY FORWARD-DIFFERENCE AND CRANK–NICOLSON METHODS

R. C. BATRA

Department of Engineering Mechanics, University of Missouri-Rolla, Rolla, MO 65401–0249, U.S.A.

AND

T. W. WRIGHT

U.S. Army Ballistic Research Laboratory, Aberdeen Proving Ground, MD 21005–0056, U.S.A.

SUMMARY

A set of non-linear and coupled equations governing the thermomechanical deformations of a viscoplastic body undergoing simple shearing deformations is integrated in time by using the forward-difference Galerkin finite-element (FDGFE) method and the Crank–Nicolson–Galerkin finite-element (CNGFE) method. In the latter scheme the number of unknown functions is increased so that the governing equations contain only first-order spatial derivatives. It is shown that the solutions obtained by the two methods agree qualitatively; however, the CNGFE method seems to introduce some damping into the system for non-polar materials, but none for dipolar materials.

INTRODUCTION

Adiabatic shear is the name given to a localization phenomenon that occurs during high-rate plastic deformation such as machining, explosive forming, shock impact loading, ballistic penetration, fragmentation, ore crushing, impact tooling failure, and metal shaping and forming processes. The localization of shear strain has been observed in steels, non-ferrous metals and polymers. The phenomenon is important in practice because progressive shearing on an intense shear band provides an undesirable mode of material resistance to imposed deformation, and the bands are often precursors of shear fracture.

A thorough study of adiabatic shear banding and processes such as metal forming, impact and penetration requires the integration, with respect to time, of a coupled system of non-linear partial differential equations. For the model representing one of these phenomena to be somewhat realistic, it should incorporate such effects as strain hardening, strain-rate hardening and thermal softening. These effects are exhibited by most metals undergoing large deformations at high strain rates. For homogeneous and simple shearing deformations of such viscoplastic materials, the adiabatic shear stress/shear strain curve is generally concave towards the origin and has a peak in it. At this peak the effect of thermal softening equals the combined effect of strain and strain-rate hardening. Under further loading, the thermal softening overtakes the strain and strain-rate hardening, and consequently the shear stress required to maintain simple shearing deformations of the body decreases with an increase in shear strain.

In nearly all the practical problems mentioned above it is necessary to integrate the governing equations well beyond the peak in the stress–strain curve. Whereas it is a trivial matter to carry out this integration when the deformations are homogeneous, it is rather time-consuming to do so for inhomogeneous deformations, even when the deformations are one-dimensional. Here we discuss our experience with two methods, the forward-difference scheme and the Crank–Nicolson method. In each case the governing partial differential equations were first reduced to a set of

0748–8025/88/060741–08$05.00

Received November 1985
Revised January 1988

ordinary differential equations by using the Galerkin finite-element method. In the Crank–Nicolson method the number of unknowns at each point was increased from five to eight so that only first-order spatial derivatives of the unknowns appeared in the equations. We should point out that the governing equations are stiff, and no artificial viscosity was introduced in either case.

Our numerical examples reveal that the Crank–Nicolson–Galerkin finite-element (CNGFE) method allows the use of timesteps at least two orders of magnitude larger than those permitted by the forward-difference Galerkin finite-element (FDGFE) scheme, and still gives an acceptable, stable solution. It is conceivable that the efficiency of the forward-difference scheme would improve if auxiliary variables were introduced, as was done for the Crank–Nicolson method, so that only first-order spatial derivatives appeared in the governing equations.

We refer the reader to excellent books[1–4] and references therein for a discussion of various numerical integration techniques. Chandra and Mukherjee[5] have recently used the forward-difference method to integrate a stiff set of partial differential equations somewhat akin to ours. They used an Euler type scheme with automatic timestep control. However, selecting parameters that control the time-increment automatically is a hard task.

In a previous paper[6] the emphasis was on reporting the complete set of solutions, obtained by using the CNGFE method, to equations studied herein. In this paper, we provide details of the two numerical techniques and compare results obtained by using the two methods.

FORMULATION OF THE SIMPLE SHEARING PROBLEM

We study the simple shearing deformations of a dipolar viscoplastic material, and assume that all the variables have been made dimensionless. Thus the body occupies the infinite slab bounded by the planes $y = \pm 1$. The governing equations (see Reference 6 for details) are

$$\dot{v} = \frac{1}{\rho}(s - l\sigma_{,y})_{,y} \tag{1}$$

$$\dot{\theta} = k\theta_{,yy} + \Lambda(s^2 + \sigma^2) \tag{2}$$

$$\dot{s} = \mu(v_{,y} - \Lambda s) \tag{3}$$

$$\dot{\sigma} = l\mu\left(v_{,yy} - \frac{\Lambda}{l}\sigma\right) \tag{4}$$

$$\dot{\psi} = \Lambda(s^2 + \sigma^2)/[1 + (\psi/\psi_0)]^n \tag{5}$$

$$\Lambda = \max\left(0, \left\{\frac{(s^2 + \sigma^2)^{1/2}}{[1 + (\psi/\psi_0)]^n(1 - a\theta)} - 1\right\}/[b(s^2 + \sigma^2)^{1/2}]\right) \tag{6}$$

with boundary conditions

$$v(\pm 1,t) = \pm 1 \tag{7}$$

$$\theta_{,y}(\pm 1,t) = 0 \tag{8}$$

$$\sigma(\pm 1,t) = 0 \tag{9}$$

and a suitable set of initial conditions. Equations (1) and (2) express, respectively, the balance of linear momentum and internal energy. Here v is the velocity of a material particle, ρ its mass density, μ its shear modulus, l a characteristic material length, k its thermal conductivity, θ its temperature change from that in the reference configuration, and s and σ may be interpreted as the shear stress and the dipolar shear stress. A superimposed dot indicates material time differentiation and a comma followed by subscript y signifies partial differentiation with respect to y. The constitutive relations (3)–(6) give one possible model of viscoplastic materials. Equation (6) implies that the plastic parts Λs and $\Lambda\sigma/l$ of the strain rate and the dipolar strain rate vanish when

$$(s^2 + \sigma^2)^{1/2} \leq [1 + (\psi/\psi_0)]^n (1 - a\theta)$$

Because variables are dimensionless, the yield stress is unity in an isothermal and quasistatic reference test. The material parameters ψ and n describe the strain hardening of the material, a is the thermal softening, and b and m represent the strain-rate sensitivity of the material.

We assume that the initial values of θ, s and ψ are symmetric in y, and those of v and σ antisymmetric in y, and seek solutions of equations (1)–(6) with the same symmetry. Thus the problem is to be studied over the spatial domain [0,1], and the boundary conditions become

$$v(1,t) = 1, \qquad v(0,t) = 0 \tag{10}$$

$$\theta_{,y}(1,t) = 0, \quad \theta_{,y}(0,t) = 0 \tag{11}$$

$$\sigma(1,t) = 0, \qquad \sigma(0,t) = 0 \tag{12}$$

For the initial conditions we take

$$v(y,0) = y, \qquad \sigma(y,0) = 0, \qquad \psi(y,0) = 0 \tag{13a}$$

$$\theta(y,0) = 0{\cdot}1(1-y^2)^9\exp^{(-5y^2)} \tag{13b}$$

$$s(y,0) = (1 - a\theta(y,0)) \tag{13c}$$

The temperature field given by equation (13b) describes the aberration in the initial temperature distribution and will result in inhomogeneous deformations of the body. Equation (13c) implies that the initial stress distribution is non-uniform and that all material points lie on their respective yield surfaces.

NUMERICAL INTEGRATION OF GOVERNING EQUATIONS

*Crank–Nicolson–Galerkin finite-element method**

With the auxiliary variables

$$u = v_{,y}, \qquad g = \theta_{,y}, \qquad p = \sigma_{,y} \tag{14}$$

we can rewrite equations (1)–(4) as

$$\dot{v} = \frac{1}{\rho}(s - lp)_{,y} \tag{15}$$

$$\dot{\theta} = kg_{,y} + \Lambda(s^2 + \sigma^2) \tag{16}$$

$$\dot{s} = \mu(u - \Lambda s) \tag{17}$$

$$\dot{\sigma} = l\mu\left(u_{,y} - \frac{\Lambda}{l}\sigma\right) \tag{18}$$

Thus only first-order spatial derivatives of the unknowns, v, θ, s, σ, u, g and p appear in the governing equations. Let H^1 denote the space of functions defined on [0,1], the square of whose first-order derivative is integrable over [0,1]. We approximate the unknown functions $v,\theta,\ldots$ by a linear combination of the finite-element basis functions $\{\phi_i(y), i=1,2,\ldots,N\}$ in an N-dimensional subspace of H^1. For example,

$$v(y,t) = v_i(t)\phi_i(y) \tag{19}$$

Throughout this paper, a repeated index implies summation over the range of the index. By using Galerkin's method[8] we thus reduce equations (14)–(18) to the following set of equations:

$$M_{ij}u_i = -Q_{ij}v_i \tag{20}$$

$$M_{ij}g_i = -\tilde{Q}_{ij}\theta_i \tag{21}$$

$$M_{ij}p_i = -Q_{ij}\sigma_i \tag{22}$$

$$M_{ij}\dot{v}_i = -\frac{1}{\rho}\tilde{Q}_{ij}s_i + \frac{l}{\rho}\tilde{Q}_{ij}p_i \tag{23}$$

* Since this paper was originally submitted the details of the CNGFE method have been published;[7] they are reproduced here for completeness.

$$M_{ij}\dot{\theta}_i = -kQ_{ij}g_i + \Lambda_i P_{ij} \tag{24}$$

$$M_{ij}\dot{s}_i = \mu M_{ij}u_i - \mu\Lambda_i s_k R_{ijk} \tag{25}$$

$$M_{ij}\dot{\sigma}_i = -\mu l\tilde{Q}_{ij}u_i - \mu\Lambda_i\sigma_k R_{ijk} \tag{26}$$

where

$$M_{ij} \equiv \int_0^1 \phi_i\phi_j dy = M_{ji} \tag{27}$$

$$Q_{ij} \equiv \int_0^1 \phi_i\phi_{j,y} dy \tag{28}$$

$$\tilde{Q}_{ij} \equiv Q_{ij} - (\phi_i\phi_j)|_0^1 \tag{29}$$

$$R_{ijk} \equiv \int_0^1 \phi_i\phi_j\phi_k \, dy = R_{ikj} = R_{kij} \tag{30}$$

$$P_{ij} \equiv \int_0^1 \phi_i\phi_j \, (s^2 + \sigma^2) dy = P_{ji} \tag{31}$$

The non-linear dependence of P_{ij} and Λ upon s, σ, ψ and θ means that the coupled set of ordinary differential equations (20)–(26) is not that easy to integrate. The matrices M_{ij}, Q_{ij}, $\tilde{Q}_{ij}$, R_{ijk} and P_{ij} have been evaluated by using the linear basis functions. Also, $v_i(t)$ denotes the velocity of node i at time t.

In the Crank–Nicolson method, equations (20)–(26), assumed to hold at time $t + \frac{1}{2}\Delta t$, are used to predict the values of v, θ, . . . at time $t + \Delta t$ from a knowledge of their values at time t. This is accomplished by approximating $\dot{\theta}_i(t + \frac{1}{2}\Delta t)$ by $(\theta_i(t + \Delta t) - \theta_i(t))/\Delta t$, $\theta_i(t + \frac{1}{2}\Delta t)$ by $\frac{1}{2}(\theta_i(t + \Delta t) + \theta_i(t))$, and so on, and by first evaluating the non-linear terms on the right-hand side of equations (20)–(26) at time t. The resulting system of linear algebraic equations is solved for $v_i(t + \Delta t)$ and similar terms, the right-hand sides of equations (20)–(26) are now evaluated at time $t + \frac{1}{2}\Delta t$, and the system of equations solved again for $v_i(t + \Delta t)$ and similar terms. This iterative process is continued until, at each nodal point,

$$|\frac{\Delta v}{v}| + |\frac{\Delta\theta}{\theta}| + |\frac{\Delta s}{s}| + |\frac{\Delta\psi}{\psi}| + |\Delta\sigma| + |\Delta g| + |\Delta p| + |\Delta u| \leq \epsilon \tag{32}$$

where the subscript i has been dropped from v_i, θ_i, . . ., Δv denotes the difference between the newly found value of v and that used to compute the right-hand side in equations (20)–(26), and ϵ is a preassigned small number. The initial conditions (13) were used to find $v_i(0)$ and similar terms.

Forward-difference Galerkin finite-element method

In this method the field equations (1) and (2) are first recast in a weak form. Let ϕ and ψ be two smooth functions defined on [0,1] such that $\phi(0) = \phi(1) = 0$. With equations (1) and (2) multiplied through by ϕ and ξ respectively, and with the boundary conditions (10)–(12), integration by parts over the interval [0,1] gives

$$\int_0^1 \dot{v}\phi dy = -\frac{1}{\rho}\int_0^1 s\phi_{,y} \, dy - \frac{l}{\rho}\int_0^1 \sigma\phi_{,yy} dy \tag{33}$$

$$\int_0^1 \theta\xi dy = -k\int_0^1 \theta_{,y}\xi_{,y} \, dy + \int_0^1 \xi\Lambda(s^2 + \sigma^2) dy \tag{34}$$

Let the interval [0,1] be divided into $N-1$ subintervals, not necessarily of equal length. Thus N is the number of nodes in the mesh. Let ϕ_i^0 and ϕ_i^1 ($i = 1,2,. . .,N$) be the Hermite basis functions,[8] and ϕ_i ($i = 1,2,. . .,N$) the finite-element basis functions introduced previously (see e.g. equation (19)). We impose the following approximations on v and θ:

$$v(y,t) = v_i(t)\,\phi_i^0(y) + \dot{\gamma}_i(t)\,\phi_i^1(y) \tag{35}$$

$$\theta(y,t) = \theta_i(t)\,\phi_i(y) \tag{36}$$

Here $\dot{\gamma}_i(t)$ is the value of $v_{,y}$ at node i at time t. Hermite basis functions ϕ_i^0 and ϕ_i^1 can be constructed by matching together element shape functions $\hat{\phi}_1^0$, $\hat{\phi}_2^0$, $\hat{\phi}_1^1$ and $\hat{\phi}_2^1$, and similarly $\phi_i(y)$ can be obtained by matching $\bar{\phi}_1$ and $\bar{\phi}_2$. In the Galerkin approximation the same set of basis functions is used to approximate the test functions ϕ and ξ as is used for v and θ. Recalling that equations (33) and (34) must hold for arbitrary ϕ and ξ, we arrive at the following set of ordinary differential equations:

$$\mathbf{M}\,\dot{\mathbf{w}} = -\mathbf{F} \tag{37}$$

$$\mathbf{H}\,\dot{\boldsymbol{\theta}} = -\mathbf{T}\boldsymbol{\theta} + \mathbf{W} \tag{38}$$

Here

$$\mathbf{w} = \{v_1, \dot{\gamma}_1, v_2, \dot{\gamma}_2, \ldots, v_N, \dot{\gamma}_N\}^{\mathrm{T}}$$

$$\boldsymbol{\theta} = \{\theta_1, \theta_2, \ldots, \theta_N\}^{\mathrm{T}}$$

$$\mathbf{F} = \{F_1, F_2, \ldots, F_{2N}\}^{\mathrm{T}} = \sum_{J=1}^{N-1} \{f_{JJ}, f_{(J+1)J}, f_{(J+2)J}, f_{(J+3)J}\}^{\mathrm{T}}$$

$$\begin{Bmatrix} f_{JJ} \\ f_{(J+1)J} \\ f_{(J+2)J} \\ f_{(J+3)J} \end{Bmatrix} = \int_{\Omega_J} \begin{Bmatrix} s\phi_{1,y}^0 + l\sigma\,\phi_{1,yy}^0 \\ s\phi_{1,y}^1 + l\sigma\,\phi_{1,yy}^1 \\ s\phi_{2,y}^0 + l\sigma\,\phi_{2,yy}^0 \\ s\phi_{2,y}^1 + l\sigma\,\phi_{2,yy}^1 \end{Bmatrix} \mathrm{d}y$$

$$\mathbf{M} = \sum_{J=1}^{N-1} \int_{\Omega_J} \begin{Bmatrix} \phi_1^0\phi_1^0 & \phi_1^1\phi_1^0 & \phi_2^0\phi_1^0 & \phi_2^1\phi_1^0 \\ \phi_1^0\phi_1^1 & \phi_1^1\phi_1^1 & \phi_2^0\phi_1^1 & \phi_2^1\phi_1^1 \\ \phi_1^0\phi_2^0 & \phi_1^1\phi_2^0 & \phi_2^0\phi_2^0 & \phi_2^1\phi_2^0 \\ \phi_1^0\phi_2^1 & \phi_1^1\phi_2^1 & \phi_2^0\phi_2^1 & \phi_2^1\phi_2^1 \end{Bmatrix} \mathrm{d}y$$

with similar definitions for **H**, **T** and **W**. In the above integrations Ω_J is the region occupied by the Jth element. These integrals are evaluated numerically by using the four-point Gauss integration rule. Explicit expressions for the matrices in equation (38) are not stated above since they are given in many books on the finite-element method (see e.g. Becker *et al.*[8]).

Equations (37), (38) and (3)–(5) are integrated with respect to time t by using the simple forward-difference method. The solution of equations (37) and (38) gives nodal values of v, $\dot{\gamma}$ and θ at the next step. From these, values of v, $\dot{\gamma}$, θ and $v_{,yy}$ at the Gauss points are calculated by using the interpolation relations (35) and (36). For each Gauss point, equations (3)–(5) are integrated to obtain the local values of s, σ and ψ at the next timestep. Because the integration scheme is only conditionally stable in the linear case, the timestep has to be kept very small; its value depends on the grid size, the material properties and the present deformations of the body.

COMPUTATION AND DISCUSSION OF RESULTS

In order to compute numerical results the following values of various dimensionless parameters that correspond to a typical hard steel were chosen: $\rho = 1{\cdot}5711\times10^{-4}$, $k = 1{\cdot}9891 \times 10^{-3}$, $a = 0{\cdot}4973$, $\mu = 240{\cdot}3$, $n = 0{\cdot}09$, $b = 10^7$ and $m = 0{\cdot}025$.

For homogeneous deformations of the block, the peak in the shear stress/shear strain curve occurs at a strain of 0·093. In solving the problem by either of the two methods, no attempt was

made to use diagonal matrices equivalent, in some sense, to those computed by using the basis functions. The domain [0,1] was divided into 13 subdomains with nodes at 0, 0·05, 0·10, 0·15, 0·20, 0·25, 0·34375, 0·43750, 0·53120, 0·6250, 0·71875, 0·81250 and 1·0. For the forward-difference scheme various integrals appearing in the expressions for **F**, **M**, **H**, **T** and W were evaluated by using the four-point Gauss quadrature rule.

When $l = 0{\cdot}0$ the forward-difference scheme necessitated taking $\Delta t = 5 \times 10^{-8}$ in order to obtain a stable solution. However, for the Crank–Nicolson method $\Delta t = 10^{-5}$ was found to give a stable and acceptable solution since the results obtained with $\Delta t = 5 \times 10^{-6}$ were found to be indistinguishable from those computed with the larger value of Δt. However, the results presented here are for $\Delta t = 5 \times 10^{-6}$.

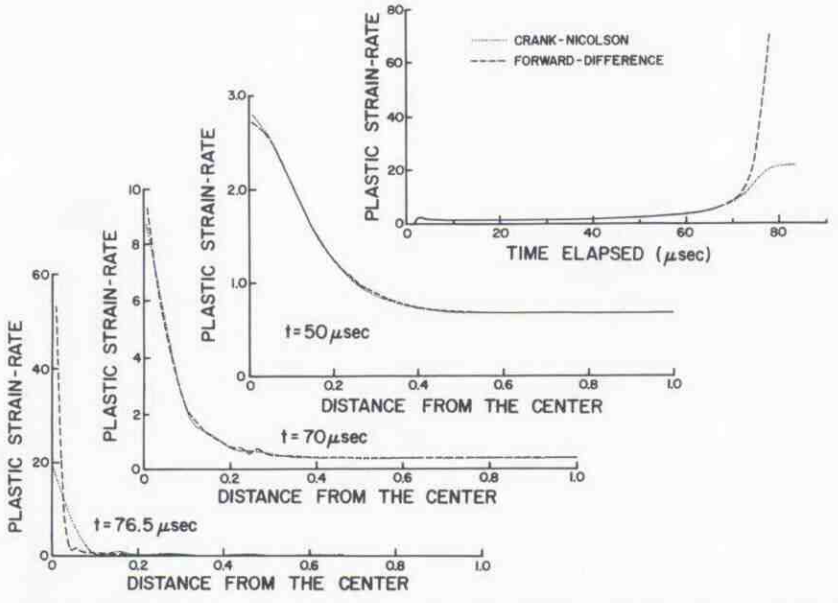

Figure 1. The evolution of the plastic strain rate at the centre of a specimen of non-polar material and its distribution within the specimen at different times

Figure 1 depicts the evolution of the plastic strain rate at the centre of a specimen of non-polar (i.e. $l = 0$) material, and the distribution of plastic strain rate within the specimen at different times. Initially the two methods give almost identical results. However, when the deformation begins to localize near the centre of the block the FDGFE method gives higher values of the plastic strain rate at points near the centre of the specimen, and also results in narrower regions of rapidly deforming material, than given by the CNGFE method. Not only is the localization delayed by the CNGFE method, but the peak value of the plastic strian rate computed is lower than that obtained by using the FDGFE method. As is discussed elsewhere,[6] the development of a late-stage plateau in the peak plastic strain rate is a numerical artifact and does not represent a physical phenomenon. The plateau was also developed in the solution computed by using the FDGFE method (although it is not shown in Figure 1). The computed results are qualitatively similar for different meshes, but differ quantitatively. The CPU time required to compute the solution by the FDGFE method was nearly three times that needed for the CNGFE method when ϵ in equation (32) was set equal to 0·01. In each case the shear stress became uniform throughout the specimen shortly after the temperature perturbation was introduced, and stayed uniform until the time for which results are presented here. The computed results for times much higher than this were not considered acceptable because the shear stress developed oscillatory behaviour, probably as a result of the coarseness of the mesh, the timestep size and/or the integration schemes used.

Figure 2 shows how the temperature at different points within the specimen evolves as the specimen is being deformed. Because of the assumption of insulated boundaries, and as heat is generated by plastic working, the temperature at every point in the material increases. As the deformation begins to localize near the centre of the specimen, the temperature at points near the centre increases considerably more than at points away from the centre. Again, the two methods give virtually identical temperature distributions until the deformation begins to localize.

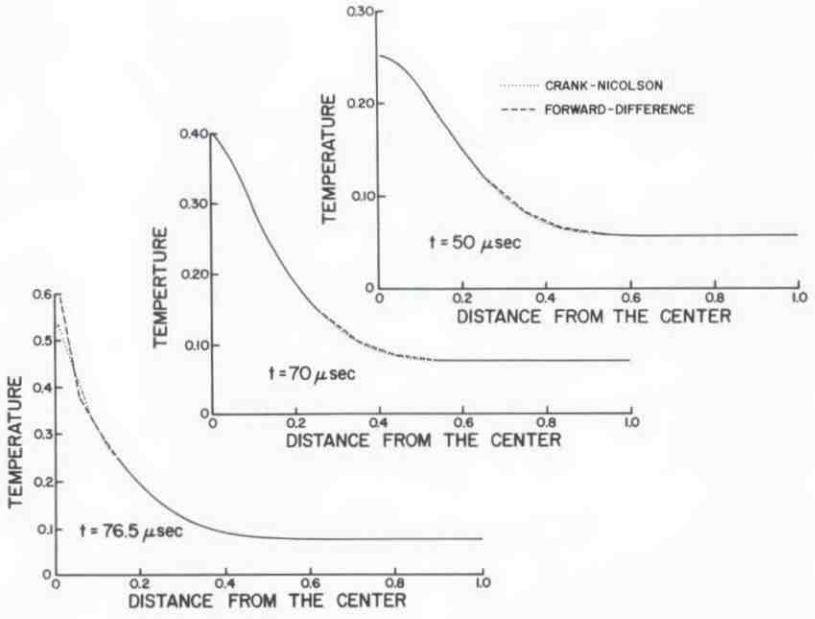

Figure 2. The distribution of the temperature within a specimen of non-polar materials at different times

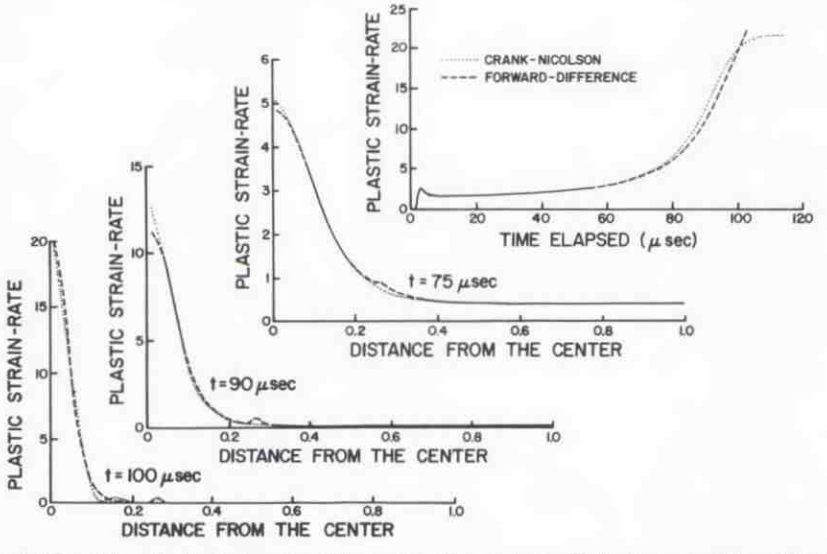

Figure 3. The evolution of the plastic strain rate at the centre of a specimen of dipolar material, and its distribution within the specimen at different times

Figure 3 compares the solutions for the dipolar materials with $l = 0{\cdot}01$. In this case the two methods predict the initiation of localization at essentially the same time, but the peak plastic strain rate given by the FDGFE method is higher than that computed by the CNGFE method. Also, the time increment needed to compute a stable solution with the FDGFE method had to be reduced to $2{\cdot}5\times10^{-8}$, thereby necessitating at least three times as much CPU time as was required for the CNGFE method. Whereas for non-polar materials the FDGFE method gave higher values of the plastic strain rate, especially at points near the centre of the specimen, for dipolar materials the CNGFE method predicted higher values of the peak plastic strain rate until the localization of the deformation began in earnest. The two methods give virtually identical values of other field quantities, such as the dipolar stress and the temperature change, until the time for which results have been computed and plotted in Figure 3.

A comparison of the results plotted in Figures 1 and 3 reveals that the inclusion of dipolar effects delays the onset of the localization of the deformation. This delay is predicted by both methods.

Whether or not the introduction of auxiliary variables in the FDGFE method will permit the use of a larger timestep remains to be seen. Also, the use of automatic timestep control as

discussed by Chandra and Mukherjee[5] may improve the efficiency of the FDGFE method. Finally, we remark that the effect of choosing different perturbations $\theta(y,0)$ and mesh size has been discussed in References 6, 7, 9 and 10.

ACKNOWLEDGEMENTS

R. C. Batra is grateful to the U.S. National Science Foundation for the financial support through grant MSM-8715952 to the University of Missouri-Rolla.

REFERENCES

1. G. F. Carey and J. T. Oden, *Finite Elements: Computational Aspects*, Vol. III, Prentice-Hall, Englewood Cliffs, NJ, 1984.
2. O. C. Zienkiewicz, *The Finite Element Method*, McGraw-Hill, New York, 1977.
3. K. J. Bathe, *Finite Element Procedures in Engineering Analysis*, Prentice-Hall, Englewood Cliffs, NJ, 1982.
4. J. N. Reddy, *An Introduction to the Finite Element Method*, McGraw-Hill, New York, 1984.
5. A. Chandra and S. Mukherjee, 'A finite element analysis of metal forming processes with thermomechanical coupling', *Int. J. Mech. Sci.*, **26**, 661–676 (1984).
6. T. W. Wright and R. C. Batra, 'Adiabatic shear bands in simple and dipolar plastic materials', in *Proc. IUTAM Symp. on Macro- and Micro-Mechanics of High Velocity Deformation and Fracture* (K. Kawata and J. Shioiri, Eds), pp. 189–201, Springer-Verlag, Berlin, 1987.
7. R. C. Batra, 'The initiation and growth of, and the interaction among, adiabatic shear bands in simple and dipolar materials', *Int. J. Plasticity*, **3**, 75–89 (1987).
8. E. B. Becker, G. F. Carey and J. T. Oden, *Finite Elements: An Introductoin*, Vol. I, Prentice-Hall, Englewood Cliffs, NJ, 1981.
9. T. W. Wright and R. C. Batra, 'The initiation and growth of adiabatic shear bands', *Int. J. Plasticity*, **1**, 205–212 (1985).
10. T. W. Wright and R. C. Batra, 'Further results on the initiation and growth of adiabatic shear bands at high strain rates', *J. Phys. (Paris)*, **46**, C5, 323–330 (1985).